

## Isosorbide-2-benzyl Carbamate-5-salicylate, A Peripheral Anionic Site Binding Subnanomolar Selective Butyrylcholinesterase Inhibitor

Ciaran G. Carolan,<sup>†</sup> Gerald P. Dillon, Denise Khan, Sheila A. Ryder, Joanne M. Gaynor, Sean Reidy, Juan F. Marquez, Mike Jones, Valerie Holland, and John F. Gilmer\*

*School of Pharmacy and Pharmaceutical Sciences, Trinity College, Dublin 2, Ireland, and School of Science, Athlone Institute of Technology, Westmeath, Ireland. <sup>†</sup>Present address: European Molecular Biology Laboratory, Hamburg 22607, Germany.*

Received October 7, 2009

Isosorbide-2-benzyl carbamate-5-benzoate is a highly potent and selective BuChE inhibitor. Meanwhile, isosorbide-2-aspirinate-5-salicylate is a highly effective aspirin prodrug that relies on the salicylate portion to interact productively with human BuChE. By integrating the salicylate group into the carbamate design, we have produced isosorbide-2-benzyl carbamate-5-salicylate, an inhibitor of high potency (150 pM) and selectivity for human BuChE over AChE (666000) and CES2 (23000). Modeling and mutant studies indicate that it achieves its exceptional potency because of an interaction with the polar D70/Y332 cluster in the PAS of BuChE in addition to pseudosubstrate interactions with the active site.

### Introduction

The enzymes acetylcholinesterase (AChE,<sup>a</sup> EC 3.1.1.7) and butyrylcholinesterase (BuChE, EC 3.1.1.8) regulate cholinergic neurotransmission. AChE activity is dominant in the normal brain (80%) and the overall CNS distribution points to a supportive role for BuChE which is mainly glial.<sup>1</sup> Nevertheless, specific localization of BuChE may be important. Individuals with the BuChE silent genotype have been reported to have subtly different cognition to the normal genotype.<sup>2</sup> The importance of BuChE in normal cholinergic processing has been underlined with the characterization of the AChE nullizygote mouse.<sup>3</sup>

In Alzheimer's disease (AD), the balance of AChE and BuChE changes. AChE has been reported to be significantly reduced in the cortex and hippocampus in post mortem AD brain slices, whereas BuChE levels in these areas is significantly increased.<sup>4</sup> Dual inhibitors such as the compound rivastigmine have shown significant clinical utility in conferring cognitive improvements. In rats, administration of the BuChE selective inhibitor cymserine caused significant increase in ACh levels (up to 300% of those recorded prior to administration).<sup>5</sup> The inhibitor caused significant improvements in the cognitive performance of aged rats using a water maze model. This was consistent with evidence of long-term potentiation (LTP) in rat brain slices. In a small

open label study, BuChE but not AChE inhibition was associated with improvements in speed, attention, and verbal memory-related functions, indicating that BuChE is important in some aspects of AD pathophysiology.<sup>6</sup> Meanwhile, slower deterioration in attention-related performance and reduced rates of cognitive decline are apparent in AD patients who have BuChE variants with reduced enzyme activity.<sup>7</sup> While BuChE inhibits amyloid fibril formation in vitro, this is not related to its enzymatic actions as a hydrolase so it is possible to envisage an inhibition strategy that would leave its putative neuroprotective role intact.<sup>8</sup> BuChE is important in drug metabolism and detoxification,<sup>9</sup> but it is also involved in lipid metabolism and regulation.<sup>10</sup> Indeed, serum BuChE activity is positively associated with obesity, cardiovascular disease, low density lipoprotein, hepatic adiposity, and diabetes mellitus type II.<sup>10a</sup> BuChE inhibition may constitute a useful strategy for regulating adiposity.

We reported previously that isosorbide-2-carbamate-5-esters, e.g., **1**, are low nanomolar selective inhibitors of BuChE relative to AChE.<sup>11</sup> The compounds show time dependent inhibition and can be classified as pseudoirreversible inhibitors. They represent a significant departure from therapeutically used carbamates (e.g., rivastigmine), which are principally related to the natural product physostigmine (Figure 1). We subsequently reported the discovery of an isosorbide-based true aspirin prodrug, isosorbide-2-aspirinate-5-salicylate, **2**.<sup>12</sup> The 5-salicylate group in **2** was shown to be an important factor in ensuring that hydrolysis by human BuChE takes place at the benzoate ester of the 2-aspirinate group of **2** rather than at the neighboring acetyl group. Compound **2** is perhaps the first true aspirin prodrug because of this productive hydrolysis. Modeling studies suggested that the hydrolysis pattern of **2** is influenced by interactions between the 5-ester group and a H-bond network involving D70/Y332 in the PAS and S79 and W82 in the midgorge

\*To whom correspondence should be addressed. Phone: +353-1-896 2795. Fax: +353-1-896 2793. E-mail: gilmerjf@tcd.ie.

<sup>a</sup> Abbreviations: AChE, acetylcholinesterase; ATCI, acetylthiocholine iodide; BTCl, butyrylthiocholine iodide; BuChE, butyrylcholinesterase; CES2, (carboxylesterase-2); DCC, dicyclohexylcarbodiimide; DTNB, 5,5'-dithiobis-(2-nitrobenzoic acid); huBuChE, human butyrylcholinesterase; ISMN, isosorbide-5-mononitrate; ISMNA, isosorbide mononitrate aspirinate; MAO, monoamino oxidase; PAS, peripheral anionic site; SAR, structure-activity relationship; TBAF, tetrabutylammonium fluoride; TBDMS, *tert*-butyldimethylsilyl; TLC, thin layer chromatography; TMS, tetramethylsilane.

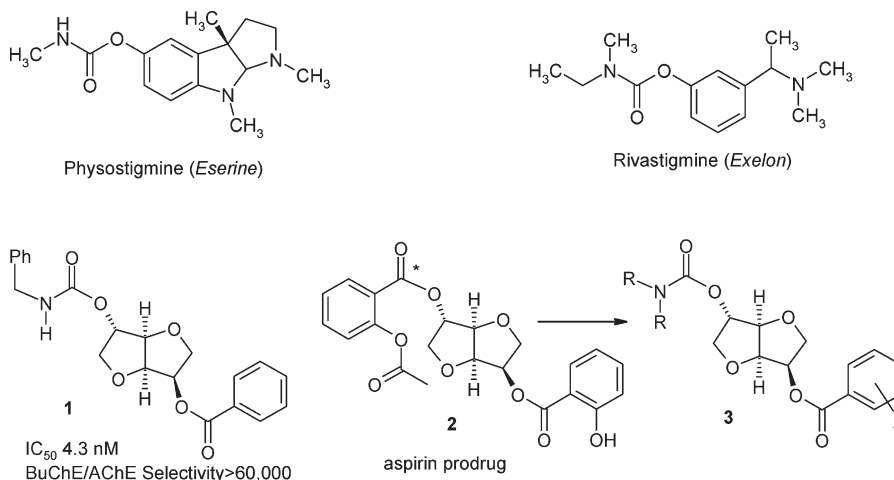


**Figure 1.** Isorbidate-based inhibitor **1**, true aspirin prodrug **2**, leading to high potency 2-carbamate-5-salicylate ester type **3**.

**Table 1.** Test Compounds along with  $IC_{50}$  Values for BuChE and % Inhibition of AChE (%I) at  $100 \mu M$

| compd         | BuChE <sup>b</sup>       |                               | AChE <sup>c</sup>   |  |
|---------------|--------------------------|-------------------------------|---------------------|--|
|               | $IC_{50}$ nM<br>(95% CI) | %I at<br>$100 \mu M$          | ratio <sup>d</sup>  |  |
| <b>5</b>      | 0.15 (0.13–0.21)         | $47 \pm 7$ (52 <sup>e</sup> ) | $> 6.6 \times 10^5$ |  |
| <b>6</b>      | 16 (14.3–18.8)           | ns <sup>a</sup>               | $> 6250$            |  |
| <b>7</b>      | 323 (251–420)            | ns                            | $> 309$             |  |
| <b>8</b>      | 18 (15–21)               | ns                            | $> 5555$            |  |
| <b>9</b>      | 32 (27–37)               | ns                            | $> 3125$            |  |
| <b>10</b>     | 117 (100–136)            | $27 \pm 2$                    | $> 854$             |  |
| <b>11</b>     | 27 (24–31)               | ns                            | $> 3703$            |  |
| <b>12</b>     | 86 (72–101)              | ns                            | $> 1166$            |  |
| <b>13</b>     | 297 (251–351)            | $33 \pm 9$                    | 336                 |  |
| <b>14</b>     | 39 (33–45)               | ns                            | $> 2564$            |  |
| <b>15</b>     | 1.2 (1.1–4.2)            | $26 \pm 2$                    | $> 83333$           |  |
| <b>18</b>     | 9.6 (7.9–11.7)           | $16 \pm 3$                    | $> 10416$           |  |
| <b>19</b>     | 6.4 (4.2–9.7)            | ns                            | $> 15625$           |  |
| <b>20</b>     | 2609 (2204–3089)         | ns                            | $> 38$              |  |
| <b>21</b>     | 1057 (871–1282)          | $12 \pm 5$                    | $> 95$              |  |
| physostigmine | 19 (15–24) <sup>f</sup>  | $53 (34–71)^f$                | 2.7                 |  |

<sup>a</sup>ns means that the estimated inhibition value was not significantly different from zero. <sup>b</sup>Measurement made with human BuChE (95% CI = 95% confidence interval). <sup>c</sup>Measurement made with electric eel AChE. <sup>d</sup>A selectivity ratio was estimated using a value of  $100 \mu M$  for AChE because the  $IC_{50}$  value was not reached at less than this. <sup>e</sup>Measurement made with human erythrocyte AChE rather than electric eel. <sup>f</sup> $IC_{50}$  values (nM).

region of BuChE.<sup>13</sup> Because the salicylate group was apparently required for specific processing of **2**, we hypothesized that introduction of similar 5-ester groups would increase inhibitory potency in the parallel isorbidate-carbamate class. One such salicylate-carbamate is a subnanomolar, highly specific inhibitor of BuChE over related esterases. It appears to achieve high potency because of binding to D70/Y332 in the PAS.

### Chemistry, Enzyme Inhibition, Selectivity, and Stability

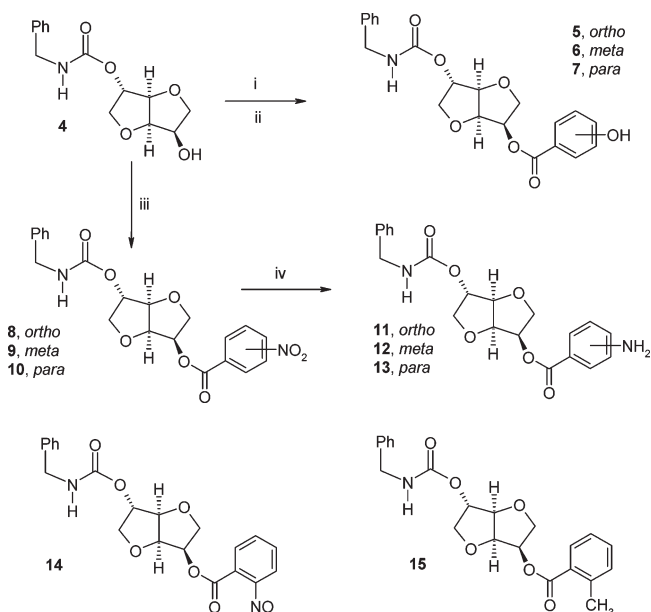
The key intermediate **4** was obtained in two steps from isorbidate mononitrate (ISMN).<sup>11</sup> It was possible to produce some of the target compounds by direct esterification of **4** with the appropriate acid chloride or with the carboxylic acid and a coupling agent. This was the case for the nitro-substituted benzoates (**8–10**) and the toluate (**15**). However, in preparing the salicylate **5** and isomers (**6–7**), it was necessary to protect

the phenolic –OH group of the hydroxybenzoic acids before esterification because of competition between the phenolic –OH and isorbidate–OH group. The relevant benzyl protected acids were obtained as described previously.<sup>12,13</sup> The amines (**11–13**) were produced by standard reduction of the nitro series (**8–10**). A substantial amount of the *ortho*-nitroso compound (**14**) was isolated from the mixture following reduction of the *ortho*-nitrobenzoate, and this was characterized and tested too. Enzyme inhibition was evaluated using Ellman's spectrophotometric determination of cholinesterase activity with either human plasma or purified BuChE from human plasma. For AChE measurements, electric eel or human erythrocyte enzyme was used as specified in Table 1. Butyrylthiocholine was used as a substrate for BuChE and acetylthiocholine as AChE substrate. Evaluations were made following 30 min incubation time, as this was shown before to allow optimal interaction between isorbidate-based inhibitors and BuChE<sup>11</sup> and because it was intended to kinetically characterize the more interesting compounds anyway.

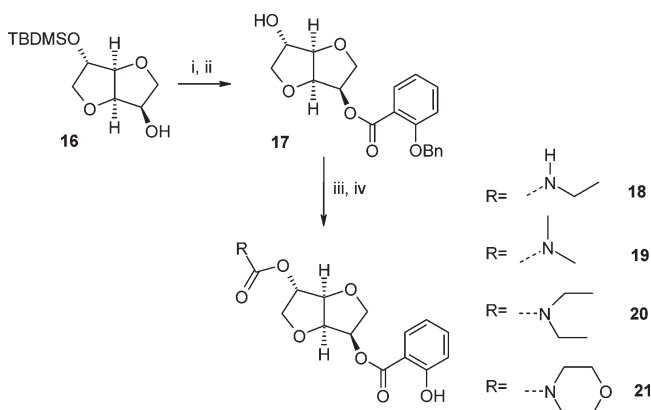
The test compounds were potent and selective inhibitors of BuChE (Table 1). The *ortho*-hydroxybenzoate (**5**) is one of the most potent cholinesterase inhibitors discovered ( $IC_{50}$  of 151 pM) and the most highly selective over AChE (BuChE/AChE  $> 500000$ ). Previously reported isorbidate-based carbamates were also highly selective toward BuChE.<sup>11</sup> Interestingly some isorbidate-diester are moderately potent mixed-mode inhibitors of AChE but exceptionally good substrates for BuChE. Kinetic and modeling data indicate that these compounds bind in the AChE gorge distal to the catalytic subsite and evidently do not interact favorably for turnover.<sup>14</sup> The diesters and analogous carbamate compounds appear to fit BuChE very well but are probably too large for processing in the smaller AChE catalytic site.

Compound **5** is 30-fold more potent than the corresponding unsubstituted-5-benzoate **1** using the 30 min  $IC_{50}$  values. This increase in potency was gratifying because it followed directly from the recognition that the salicylate group in the aspirin prodrug series (**2**) promotes productive interactions with BuChE. For example, isorbidate-2-aspirinate-5-salicylate is a far more efficient aspirin prodrug than its 5-benzoate analogue, which is hydrolyzed largely at the acetyl group, producing the isorbidate-2-salicylate-5-benzoate.<sup>13</sup>

The isomeric *meta*- and *para*-hydroxybenzoates **6** and **7** were significantly less potent than **5** (16 and 323 nM, respectively). Equally, as reported, the *meta* and *para*-hydroxy

**Scheme 1.** Showing Preparation of 2-Benzylcarbamate-5-Substituted Benzoates

(i)  $\text{BnOPhC(O)OH}$ , DCC, DMAP, DCM, RT, 8 h; (ii) Pd/C,  $\text{H}_2$ , EtOAc, 12 h, RT; (iii)  $\text{NO}_2\text{PhC(O)Cl}$ ,  $\text{Et}_3\text{N}$ , DCM, RT, 8 h or  $\text{NO}_2\text{PhC(O)OH}$ , DCC, DMAP, DCM, RT, 8 h; (iv)  $\text{H}_2$ , Pd/C, MeOH:EtOAc, 24 h, RT.

**Scheme 2.** Showing Preparation of 5-Salicylate-2-alkyl Carbamates

(i) Benzylprotected salicylic acid, DCC, DMAP, DCM, RT, 8 h; (ii) TBAF, DCM, RT, 15 min; (iii) carbamoyl chloride, pyr, 80 °C, 24 h; (iv)  $\text{H}_2$ , Pd/C, MeOH:EtOAc, 24 h, RT.

benzoates are not as effective as aspirin prodrugs as the ortho compounds.<sup>13</sup> This general pattern in the inhibitor class was followed by the analogous nitro- and aminobenzoates (**8–10**). The *ortho*-toluate (**15**) was also a highly potent compound.

As the salicylate **5** exhibited such exceptional potency, we decided to examine the effect of replacement of the 2-benzylcarbamate group with other carbamate groups while maintaining the 5-salicylate ester. In our earlier work, we had shown that in the isosorbide-based compounds, phenyl carbamates tend not to be potent BuChE inhibitors, indeed they are moderately potent AChE inhibitors.<sup>11</sup> We therefore decided to examine a small panel of primary and secondary alkyl carbamates. In preparing these, it was necessary to introduce the benzyl protected salicylate first followed by

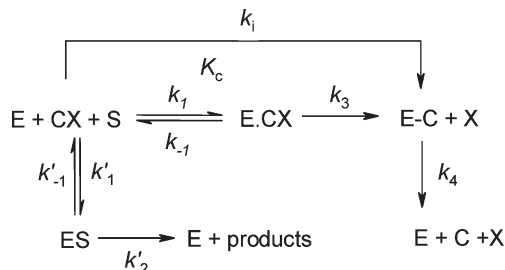


**Figure 2.** Inhibition of BuChE enzyme (E) by carbamates CX begins with a reversible interaction forming the complex E.CX, which is analogous to the Michaelis complex ( $K_c$ ) in enzyme substrate processing. This is followed by carbamylation, which has a unimolecular rate constant  $k_3$ . The overall carbamylation event is characterized by the second-order rate constant  $k_i$ , which can be estimated from  $k_3/K_c$ .  $k_4$  represents the rate of recovery of enzyme activity. Decarbamylation kinetics following inhibition by isosorbide benzyl- and butyl-carbamate inhibitors was shown to be very slow previously and can be ignored if the initial phase of the reaction is monitored.<sup>15</sup>

carbamylation and deprotection (Scheme 2). Isosorbide-2-TBDMS (**15**) was obtained from ISMN in two steps and esterified with benzyl-protected salicylic acid. The 2-OH was deprotected (TBAF), carbamylated with the appropriate primary or secondary carbamyl chloride, and the salicylate-OH group deprotected ( $\text{H}_2$ , Pd/C). The dimethyl and ethyl-carbamate (**18**, **19**) were potent inhibitors of BuChE ( $\text{IC}_{50} < 10$  nM), but the morpholine and diethylcarbamate compounds (**20**, **21**) were micromolar inhibitors. There was a 270-fold difference in potency between the ethyl (**18**,  $\text{IC}_{50}$  9.6 nM) and diethyl carbamate (**20**,  $\text{IC}_{50}$  2.6  $\mu\text{M}$ ). This appears to be due to steric reasons rather than loss of interactions with the carbamate NH because the dimethyl compound (**19**) was equipotent ( $\text{IC}_{50}$  6.4 nM) with **18**.

We also studied the effect of **5** on two closely related carboxylesterase enzymes human carboxylesterase-1 (CES1) and carboxylesterase-2 (CES2) present in hepatocyte and intestinal enterocyte microsomes respectively using *para*-nitrophenyl acetate (*p*NPA) as substrate.<sup>15</sup> CES-1 and -2 have high homology and sequence identity with BuChE (40–50%), and they too are involved in drug metabolism and prodrug activation. However, they are markedly less efficient at processing positively charged esters such as choline esters and therefore classical amino-inhibitors tend to be selective toward the cholinesterases. Compound **5** was not an inhibitor of *p*-NPA turnover by human hepatic CES-1 but it was moderately potent toward CES-2 ( $\text{IC}_{50} = 3.42 \pm 1.18 \mu\text{M}$ ; BuChE/CES-2 selectivity 22800).

Another factor likely to influence the distribution and potential utility of **5** is the vulnerability of its 5-salicylate ester group toward nonspecific hydrolysis. The stability of **5** was therefore evaluated in human plasma solution (33–50%), mouse plasma (33%), and mouse liver homogenate. Remaining ester ( $1 \times 10^{-4}$  M) as a function of time was determined using HPLC. There was no evidence of hydrolysis in any of these matrices over the course of 1 h.

**Enzyme Inhibition Kinetic Studies**

To investigate the reasons for the increased potency of **5** and its ethyl carbamate analogue **18** relative to the unsubstituted benzoates, we undertook detailed enzyme inhibition studies with some of the key compounds including **5**, the toluate **15**, **18**, and related compounds whose  $\text{IC}_{50}$  values we had reported

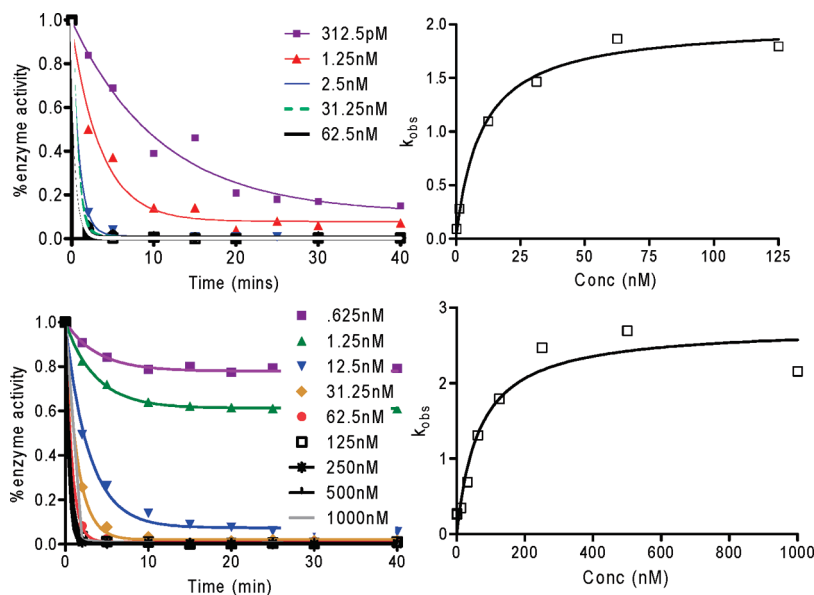


**Figure 3.** First-order decay curves for (a) the inhibition of WT BuChE by compound **5** (312 pM–62.5 nM); (b) inhibition of the D70G BuChE mutant by compound **5** (625 pM–1  $\mu$ M). A value of  $k_{obs}$ , the observed rate constant for inhibition, was calculated from each curve in these plots and plotted against concentration as shown in the second column below.

previously; the benzoate **1**, 2-butylcarbamate-5-benzoate (**22**), the unsubstituted isosorbide-2-benzyl carbamate (**4**), 2-benzylcarbamate-5-nicotinate (**23**), and 2-benzylcarbamate-5-biphenylester (**24**). For comparison, we included also the clinically used rivastigmine and the classical agent physostigmine (eserine) (Figure 1).

Carbamate inhibition of cholinesterases occurs through initial reversible interaction followed by carbamylation of the serine of the catalytic triad (Figure 2).<sup>16a-c</sup> Decay of enzyme activity follows apparent first-order kinetics when the inhibitor concentration [CX] is higher than that of the enzyme [E]. The rate of carbamylation of the enzyme ( $k_{obs}$ ) can be estimated by measuring residual enzyme activity at intervals following mixing of enzyme and inhibitor (Figure 3):

$$R = R_0 e^{-k_{obs} \cdot t} + R_{\infty} \quad (1)$$

where  $R$ ,  $R_0$ , and  $R_{\infty}$  are ratios of the inhibited enzyme activity ( $v_t$ ) to the control activity ( $v_0$ ) at times  $t$ , 0, and,  $t_{\infty}$ , respectively.<sup>16</sup> Plots of  $k_{obs}$  versus inhibitor concentration follows a rectangular pseudo Michaelis Menten curve from which it was possible to estimate  $K_c$ , which characterizes the initial equilibrium and  $k_3$  the unimolecular carbamylation rate constant:

$$k_{obs} = \frac{k_3 [CX]}{K_c (1 + [S]/K_m) + [CX]} \quad (2)$$

The  $K_c$  value can be interpreted as reflecting the affinity between inhibitor and cholinesterase resulting from topological or electronic complementarity: the  $k_3$  value, the maximum velocity of carbamylation (Figure 2). The second-order rate constant  $k_1$  ( $= k_3/K_c$ ) is a measure of overall carbamylation efficiency. We adopted this approach in order to separate out the successive phases of the reaction and to determine the basis for the differences in 30 min  $IC_{50}$  values potency already observed (Table 2).  $K_c$  values were lowest for the salicylates **5** and **18**. They were also lower for the 2-benzyl carbamate than

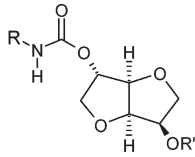
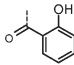
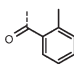
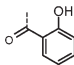
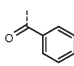
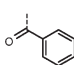
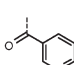
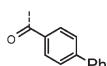
for corresponding ethyl- and butyl- compounds (**5/18**, **1/22**). Compound **5** exhibited the greatest intrinsic affinity as reflected in its low nanomolar  $K_c$  value, and it had the highest overall carbamylation efficiency ( $k_1 = 201 \mu\text{M}^{-1} \cdot \text{min}^{-1}$ ). The  $K_c$  values for **5** and the unsubstituted benzoate **1** imply that the simple introduction of the salicylate-OH group increases enzyme affinity 100 fold. Carbamylation rate constants were similar across the series apart from two cases, the weak inhibitor **4** and the potent biphenylester **24**, which is probably explained by its size and slower diffusion speed. Comparison of the latter with the nicotinate **23** is instructive. These two compounds are similar in 30 min  $IC_{50}$  values and overall carbamylation efficiencies (1.5), however, **23** has relative to **24** a high  $k_3$  but significantly lower intrinsic affinity ( $K_c$ ). Therefore its potency arises because its affinity compensates for its slower chemistry. Overall though, there was a significant correlation between  $K_c$  and 30 min  $IC_{50}$  ( $r^2 = 0.85$ ). Values for  $k_5$ , the decarbamylation reaction, were estimated for the potent compounds **5** and rivastigmine (Figure 1). Enzyme recovery was initiated by diluting inhibited enzyme 1000-fold, and the rate of recovery was monitored over an extended period of time thereafter. Recovery of enzyme activity followed first-order curves in each case from which values of  $0.32 \text{ h}^{-1}$  and  $2.76 \text{ h}^{-1}$  were obtained for **5** and rivastigmine, respectively. Clearly, the benzyl carbamate adduct resulting from carbamylation with **5** is stable for relatively long periods compared to the adduct generated by rivastigmine. This could be due to its intrinsic stability or to suppression of its hydrolysis by the leaving group. Leaving group effects on BuChE decarbamylation are not well characterized, but the phenomenon has been reported for AChE.<sup>17</sup>

### Modeling of Carbamate Binding to BuChE

The crystal structures of the cholinesterase enzymes, both in their apo- forms and in complex with a variety of ligands, have been published,<sup>18-21</sup> and the structural basis of substrate and inhibitor processing is well understood. To investigate the reasons for the marked increase in potency associated with salicylate compounds, the test compounds were docked to the



**Table 2.** Kinetic Values for Enzyme Carbamylation of WT Human BuChE<sup>a</sup>

|  |    |   | $K_c$         | $k_3$                 | $k_i$                                      | $k_5$               |
|---|----|---|---------------|-----------------------|--|---------------------|
|   |    |   | $\mu\text{M}$ | ( $\text{min}^{-1}$ ) | ( $\mu\text{M}^{-1}\cdot\text{min}^{-1}$ ) | ( $\text{h}^{-1}$ ) |
| Cpd (IC <sub>50</sub> )   | R  | R'  |               |                       |  |                     |
| <b>5</b> (151 pM)   | Bn |    | 0.010±0.002   | 2.01±0.09             | 201.0                                      | 0.32±0.04           |
| <b>15</b> (1.2 nM)  | Bn |    | 0.248±0.060   | 1.85±0.10             | 7.45                                       |                     |
| <b>18</b> (6.4 nM)  | Et |    | 0.075±0.013   | 1.84±1.02             | 24.5                                       |                     |
| <sup>†</sup> <b>4</b> (3.7 μM)  | Bn | H   | 18.7±11.5     | 0.14±0.04             | 0.008                                      |                     |
| <sup>†</sup> <b>1</b> (4.3 nM)  | Bn |    | 0.90±0.47     | 3.01±0.45             | 3.34                                       |                     |
| <sup>†</sup> <b>22</b> (72 nM)  | Bu |    | 2.57±0.40     | 2.62±0.16             | 1.02                                       |                     |
| <sup>†</sup> <b>23</b> (57 nM)  | Bn |   | 1.90±0.20     | 2.69±0.16             | 1.41                                       |                     |
| <sup>†</sup> <b>24</b> (12 nM)  | Bn |  | 0.40±0.01     | 0.62±0.05             | 1.53                                       |                     |
| Physostigmine (19 nM)   |    |   | 0.41±0.09     | 2.76±0.17             | 6.75                                       |                     |
| Rivastigmine (37 nM <sup>‡</sup> )  |    |   | 4.04±1.34     | 2.41±0.15             | 0.59                                       | 2.76±1.80           |

<sup>a</sup> Values given ± SEM: <sup>†</sup> IC<sub>50</sub> values from ref 11, <sup>‡</sup> from ref 27.

BuChE active site gorge using Autodock,<sup>22</sup> which has provided accurate results for ligand binding to cholinesterase enzyme in the past.<sup>23,24</sup> Models of the test compounds were flexibly docked in a model of BuChE based on the X-ray crystal structure, with some key residues allowing flexibility (depicted in Figures 4 and 5 for **5** and **18**). The highest scoring poses in each case could be interpreted as Michaelis complexes, with the isosorbide group close to the base of the gorge, the carbamate in the acyl pocket, and the serine oriented for attack close to the carbonyl carbonyl. The poses were overall similar across the family of compounds. There are at least two possible explanations for the ortho effect observed. First, the ortho-substituted compounds are subject to intramolecular bonding between the phenyl substituent and the carbonyl oxygen of the ester group. The “ortho effect” is most apparent for the salicylate compound **5** and the amino-substituted compound **11**. In both cases, an intramolecular hydrogen bond exists between the substituent at the ortho position and the carbonyl oxygen of the ester group in the enzyme bound models. The interaction is prominent in the <sup>1</sup>H NMR spectra of the compounds in chloroform. This bond could act as a preselection mechanism, preorganizing the ligand so that the phenyl ring is planar with the partner indole

system of W82. As a result, there is a less significant loss of entropy associated with binding of these ligands compared to those substituted at the meta and para positions.

Notably, the modeling indicated potentially significant interactions between the salicylate—OH group and members of the PAS and H-bonded in the wild type BuChE. The BuChE PAS plays a key role in initial substrate binding and steering and in the excess characteristic substrate activation of BuChE being dynamically linked through the Ω loop to W82 of the cation—π site.<sup>25,26</sup> As shown in Figures 4 and 5, the *ortho*-hydroxyl group of compounds **5** and **18** can hydrogen-bond to the side chains of D70 and Y332 and, upon 180° rotation of the benzene ring about its axis, with the OH group of Y440. The position of the —OH group ortho to the benzene ring appears optimal for such interactions across the whole 360° rotation about its axis. The aromatic PAS of AChE catalyzes the assembly of amyloid fibrils *in vitro*; normal substrate interactions there are associated with inhibition of turnover. BuChE-selective inhibitors have been reported to reduce Aβ and APP secretion *in vitro* and *in vivo*, but it is not clear if the BuChE PAS is involved in this.<sup>5</sup> The acyl pocket of the enzyme is large but relatively narrow, framed as it is by residues L286 and V288. The benzyl group occupies it especially well (Figure 4).

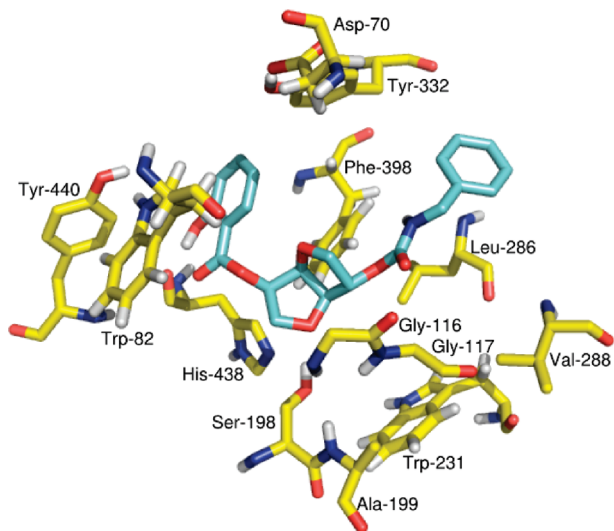


**Figure 4.** Binding of isosorbide 2-benzyl carbamate 5-salicylate (**5**) to *hu*BChE, as predicted by docking the ligand to the crystal structure using Autodock 4. With the carbamate moiety suitably poised for interaction with the enzyme's catalytic machinery, the ligand is in an orientation in which the  $-OH$  group of the 5-salicylate can interact with Y440, or by rotation about the axis of the aromatic ring, with D70 and Y332. Such interactions stabilize the ligand in the orientation indicated, increasing the rate of Michaelis complex formation and, thus, the rate of overall enzyme inhibition.

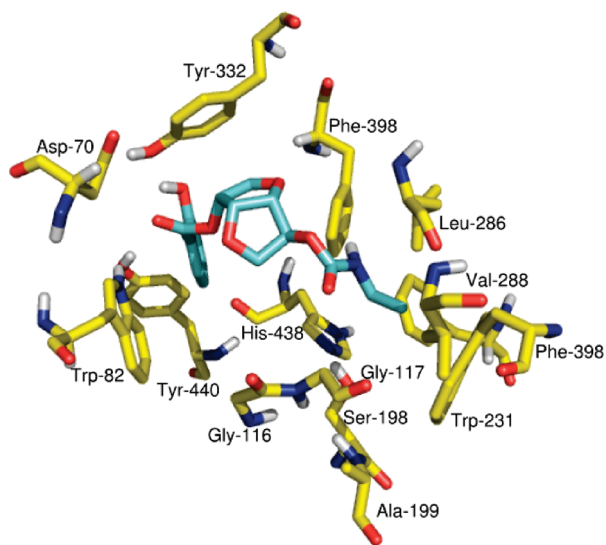


**Figure 5.** Binding of isosorbide 2-ethyl carbamate 5-salicylate (**18**) to *hu*BChE, as predicted by docking the compound to the crystal structure of the enzyme using the Autodock program. With the carbamate functionality oriented toward Ser-198 as required for enzyme carbamylation, the hydroxyl group of the ligand's salicylate moiety can interact with D70 and Y332 at the peripheral site of BuChE, strengthening interactions and increasing the rate of enzyme inhibition.

Smaller methyl and ethyl groups (compounds **18** and **19**) are easily accommodated but form less productive contacts with surrounding residues on account of their smaller size (e.g., Figure 5). Disubstituted carbamates larger than methyl are too large to fit in the pocket, and thus compounds **20** and **21** are poor inhibitors of BuChE.

### Mutant Studies

Modeling suggested that the increased binding affinity, reflected in lower  $K_c$  values (Table 2) could be attributed to specific associations between the OH group of **5** and **18** and a H-bond network encompassing PAS residues D70 and Y332. We studied the kinetics of inhibition by selected carbamate inhibitors with D70G and Y332A mutants as well as a D70G/Y332A double mutant (Table 3). The salicylate compound **5** bound less avidly to the mutant enzymes as reflected in significant increase in  $K_c$  ( $K_c$  9.9/445 nM). Similarly, compound **18** preferentially binds the wild type enzyme compared to the mutant enzymes, which can also be attributed to loss of specific associations with the mutated residues. The contrast with the results from the benzoate compounds **1** and **22**, which lack the important *ortho*-hydroxyl group, is notable—while the benzoate **1** does form less favorable contacts with the mutant enzymes than the wild type enzyme (indicating that the peripheral site residues are important for general ligand binding), the difference in  $K_c$  values between wild type and mutant enzymes is much less significant for **1** and **22** than for the salicylate compounds **5** and **18**.

To examine the extent to which specific interactions might be responsible for some of the improvement in inhibitor binding observed when the inhibitors interact with wild type compared to mutant enzymes, we examined the free energies of binding for each ligand to the enzymes. The change in free energy of initial binding caused by mutations,  $\Delta\Delta G_{\text{mut-wt}}$  was calculated according to the following equation:

$$\Delta\Delta G_{\text{mut-wt}} = -RT \ln(K_{c(\text{mut})}/K_{c(\text{wt})})$$

where  $K_{c(\text{mut})}$  and  $K_{c(\text{wt})}$  are the dissociation constants for Michaelis complex formation in the mutant and wild-type enzymes respectively.  $R$  is the gas constant ( $1.99 \times 10^{-3}$  kcal $\cdot$ mol $^{-1}\cdot$ K $^{-1}$ ), and  $T$  was taken as 310 K.  $\Delta G$  of wild type BChE was taken as a reference value.

For compound **5**, the values of  $\Delta\Delta G$  for binding to the D70G and Y332A mutants were thus found to be  $-1.17$  kcal $\cdot$ mol $^{-1}$  and  $-1.00$  kcal $\cdot$ mol $^{-1}$ , respectively. In the double mutant, the calculated value was  $-2.35$  kcal $\cdot$ mol $^{-1}$ . The values are almost but not quite additive, suggesting that conformational changes associated with the double mutation contribute to reduced affinity for the ligand as well as the loss of contacts with the ligand shown in the models previously. For the ethyl carbamate 5-salicylate compound (**18**), the values of  $\Delta\Delta G$  for binding to the D70G and Y332A mutants were calculated as  $-0.89$  and  $-1.06$  kcal $\cdot$ mol $^{-1}$ , respectively,

**Table 3.** Kinetic Values for Interaction with Mutant BuChE Enzymes

|           | $K_c$<br>( $\mu\text{M}$ ) |                   |                   | $k_3$<br>( $\text{min}^{-1}$ ) |               |               |
|-----------|----------------------------|-------------------|-------------------|--------------------------------|---------------|---------------|
|           | D70G                       | Y332A             | D70G/Y332A        | D70G                           | Y332A         | D70G/Y332A    |
| <b>5</b>  | $0.067 \pm 0.021$          | $0.050 \pm 0.006$ | $0.445 \pm 0.106$ | $2.7 \pm 0.2$                  | $2.7 \pm 0.2$ | $3.1 \pm 0.1$ |
| <b>1</b>  | $2.4 \pm 1.3$              | $1.5 \pm 0.7$     | $6.4 \pm 3.1$     | $3.6 \pm 0.9$                  | $1.3 \pm 0.2$ | $2.0 \pm 0.4$ |
| <b>18</b> | $0.32 \pm 0.04$            | $0.42 \pm 0.06$   | $2.26 \pm 0.40$   | $2.5 \pm 0.1$                  | $2.9 \pm 0.1$ | $2.3 \pm 0.2$ |
| <b>22</b> | $2.7 \pm 0.6$              | $1.3 \pm 1.1$     | $5.3 \pm 0.9$     | $2.6 \pm 0.2$                  | $1.3 \pm 0.6$ | $1.7 \pm 0.1$ |

and in the double mutant,  $-2.10 \text{ kcal} \cdot \text{mol}^{-1}$ . By comparison, values of  $-0.60$ ,  $-0.31$ , and  $-1.21 \text{ kcal} \cdot \text{mol}^{-1}$  were calculated for the benzoate compound **1**. The loss in free energy of binding of the benzoate compound upon mutation of the peripheral site residues is much less significant than that for the salicylate compounds, suggesting that the proposed interactions between the salicylate  $-\text{OH}$  group and the side chains of those residues are important. The mutant enzymes have different conformations compared to the wild type enzyme, and the hydration state of the active site gorge may change upon mutation.<sup>28</sup> These phenomena may explain some of the decreased binding to mutant enzymes observed for our ligands; however, the direct hydrogen-bonding interactions proposed in our molecular models provide an attractive explanation for the marked effect of peripheral site mutation on inhibitor potency.

## Conclusion

Substrates are not always suitable templates for the design of inhibitors because of the differing geometric and electronic demands for processing and inhibition. In this study, we have designed a subnanomolar inhibitor based directly on the aspirin prodrug **2**. Contributions from peripheral or midgorge interactions to the enhanced potency were demonstrated as feasible using modeling and supported by mutant studies. These kinds of interactions have previously been shown to be important in reinforcing binding and affinity in AChE inhibitor types, but they clearly have utility in the design of inhibitors for the less explored but potentially important target BuChE. Compound **5** is one of the most potent cholinesterase inhibitors discovered, and it is the most selective. It has significant potential in biochemical and pharmacology studies delineating the role and therapeutic value of BuChE as a target in human disease.

## Experimental Section

**Synthesis.**  $^1\text{H}$  and  $^{13}\text{C}$  spectra were recorded at  $27^\circ\text{C}$  on a Bruker DPX 400 MHz FT NMR spectrometer (400.13 MHz  $^1\text{H}$ , 100.61 MHz  $^{13}\text{C}$ ) or a Bruker AV600 (600.13 MHz  $^1\text{H}$ , 150.6 MHz  $^{13}\text{C}$ ) in either  $\text{CDCl}_3$  or  $(\text{CD}_3)_2\text{CO}$  with tetramethylsilane (TMS) as internal standard. In  $\text{CDCl}_3$ ,  $^1\text{H}$  spectra were assigned relative to the TMS peak at 0.0 ppm, and  $^{13}\text{C}$  spectra were assigned relative to the middle  $\text{CDCl}_3$  triplet at 77.00 ppm. In  $(\text{CD}_3)_2\text{CO}$ ,  $^1\text{H}$  spectra were assigned relative to the  $(\text{CD}_3)_2\text{CO}$  peak at 2.05 ppm and  $^{13}\text{C}$  spectra were assigned relative to the  $(\text{CD}_3)_2\text{CO}$  at 29.5 ppm. Coupling constants were reported in hertz (Hz). HRMS was performed using a Micromass mass spectrophotometer with electrospray ionization at the School of Chemistry, Trinity College Dublin. Elemental analyses were performed at the Microanalytical Laboratory, Department of Chemistry, University College Dublin. Flash chromatography was performed on Merck Kieselgel (particle size: 40–60  $\mu\text{m}$ ). Thin layer chromatography (TLC) was performed on silica gel Merck F-254 plates. Compounds were visually detected by UV absorbance at 254 nm or with potassium permanganate or vanillin staining solution. Enzyme activity and inhibition assays were performed using an Anthos bt2 plate reader with UV detection at 412 nm. Purity was determined by elemental analysis or RP-HPLC. All test compounds were >95% pure by HPLC and/or elemental analysis.

**General Procedure (GP1) for the Synthesis of Hydroxybenzoyl Esters of 2-(Benzylaminocarbonyloxy)-1,4:3,6-dianhydro-D-glucitol.** Appropriate benzoyloxy-benzoic acid (2.1907 mmol, 500 mg) was dissolved in chloroform (20 mL) in a 100 mL round-bottom flask and cooled to  $-20^\circ\text{C}$  in a Dewar flask. To this was

added 1 mol equiv of 2-(benzylaminocarbonyloxy)-1,4:3,6-dianhydro-D-glucitol **4** (1 equiv), 1.1 mol equiv of DCC (497.2 mg), and DMAP (294.4 mg). The mixture was stirred overnight while the reaction vessel was allowed to return to room temperature. The organic solvent was evaporated under vacuum, DCM (10 mL) was added, and the urea precipitate was collected by filtration. The filtrate was washed with 1 M HCl (20 mL), 5%  $\text{NaHCO}_3$  (20 mL) saturated brine solution (20 mL), and dried over anhydrous sodium sulfate (1 g). The solution was filtered into a round-bottom flask and evaporated under vacuum. The product was dissolved in ethyl acetate/methanol (1:1, 20 mL). A spatula tip-full of 10% palladium on activated carbon was added. Air was expelled from the flask and the mixture kept under an atmosphere of  $\text{H}_2$  and stirred for 24 h. TLC showed the formation of a single product. The palladium catalyst was removed by filtration and the solvent evaporated under vacuum. The crude product was dissolved in DCM and purified by flash chromatography.

**General Procedure 2 (GP2).** To a solution of 2-(benzylaminocarbonyloxy)-1,4:3,6-dianhydro-D-glucitol **4** (1 equiv) in anhydrous DCM was added anhydrous triethylamine (1.1 equiv), followed by carboxylic acid chloride (1.1 equiv). The reaction mixture was left stirring for 12 h under a nitrogen atmosphere with the absence of light. The reaction mixture was then washed successively with 1 M HCl, saturated  $\text{NaHCO}_3$  (aq), water, and brine. The solution was then dried with  $\text{Na}_2\text{SO}_4$ , filtered, and solvent removed under reduced pressure.

**General Procedure 3 (GP3).** 2-(Hydroxyl)-5-*O*-(*o*-benzyl-oxybenzoyl)-1,4:3,6-dianhydro-D-glucitol, **17** (1 equiv), was dissolved in anhydrous pyridine and an excess of appropriate carbamoyl chloride was added. The reaction mixture was heated to  $120^\circ\text{C}$  for 24 h and kept under an atmosphere of nitrogen. The mixture was evaporated to dryness under high vacuum to remove pyridine, and the residue was diluted with DCM (20 mL) and washed with water ( $3 \times 20 \text{ mL}$ ). The organic layer was dried over anhydrous sodium sulfate (2 g) and evaporated to dryness. Purification by column chromatography afforded pure title compound.

**2-(Benzylaminocarbonyloxy)-5-*O*-Salicyloyl-1,4:3,6-dianhydro-D-glucitol (5).** 2-Benzoyloxy-benzoic acid (2.19 mmol, 500 mg) and 2-(benzylaminocarbonyloxy)-1,4:3,6-dianhydro-D-glucitol **4** (1.22 g) were reacted according to GP1 to give the title compound as a white crystalline product after flash chromatography using hexane and ethyl acetate (1:1) as eluent (485.5 mg, 55.5%); mp  $120^\circ\text{C}$ .  $^1\text{H}$  NMR  $\delta$  ( $\text{CDCl}_3$ ): 3.94–4.10 (m, 4H), 4.34–4.42 (d, 2H,  $J = 6.02 \text{ Hz}$ ), 4.56 (d, 1H,  $J = 5.02 \text{ Hz}$ ), 4.96 (t, 1H,  $J = 5.27 \text{ Hz}$ ), 5.12 (t, 1H,  $J = 5.27 \text{ Hz}$ ), 5.22 (d, 1H,  $J = 3.01 \text{ Hz}$ ), 5.42 (dd, 1H,  $J = 5.52$  and  $10.04 \text{ Hz}$ ), 6.89–6.96 (m, 1H), 7.01 (dd, 1H,  $J = 1.01$  and  $8.54 \text{ Hz}$ ), 7.23–7.40 (m, 5H), 7.51 (m, 1H), 7.89 (dd, 1H,  $J = 1.5$  and  $8.03 \text{ Hz}$ ), 10.60 (s, 1H).  $^{13}\text{C}$  NMR ppm ( $\text{CDCl}_3$ ): 44.7, 70.3, 73.2, 74.4, 77.9, 80.5, 85.8, 111.4, 117.2, 118.8, 127.1, 127.2, 128.3, 129.5, 135.6, 137.6, 154.7, 161.2, 168.9.

**2-(Ethylaminocarbonyloxy)-5-*O*-(*o*-Benzoyloxy benzoyl)-1,4:3,6-dianhydro-D-glucitol.** Compound **17** (0.5612 mmol, 200 mg) and ethyl carbamoyl chloride were reacted according to GP3. Purification by column chromatography, using ethyl acetate and hexane (3:1, 2:1, 1:1) as eluent, yielded the target compound as a colorless oil (153.8 mg, 64.1%).  $^1\text{H}$  NMR  $\delta$  ( $\text{CDCl}_3$ ): 1.14 (t, 3H,  $J = 7.28 \text{ Hz}$ ), 3.21 (m, 2H), 3.87 (dd, 1H,  $J = 5.52$  and  $10.04 \text{ Hz}$ ), 3.91–4.03 (m, 3H), 4.53 (d, 1H,  $J = 4.51 \text{ Hz}$ ), 4.83 (s, 1H), 4.93 (t, 1H,  $J = 5.02 \text{ Hz}$ ), 5.12 (s, 1H), 5.19 (s, 2H), 5.37 (dd, 1H,  $J = 5.52$  and  $11.54 \text{ Hz}$ ), 6.98–7.07 (m, 2H), 7.27–7.54 (m, 6H), 7.90 (dd, 1H,  $J = 2.01$  and  $8.03 \text{ Hz}$ ).  $^{13}\text{C}$  NMR ppm ( $\text{CDCl}_3$ ): 14.7, 35.4, 69.9, 70.1, 73.1, 73.9, 77.8, 80.3, 85.7, 113.2, 119.3, 120.1, 126.7, 127.5, 128.1, 131.8, 133.4, 136.1, 154.7, 157.9, 165.2.

**2-(Ethylaminocarbonyloxy)-5-*O*-Salicyloyl-1,4:3,6-dianhydro-D-glucitol (18).** Hydrogenation of its benzyl protected precursor in the presence of palladium on carbon gave **18** as a white



crystalline product (69.4 mg, 58.6%); mp 118 °C.  $^1\text{H}$  NMR  $\delta$  ( $\text{CDCl}_3$ ): 1.14 (t, 3H,  $J = 7.28$  Hz), 3.19 (m, 2H), 3.92–4.10 (m, 4H), 4.55 (d, 1H,  $J = 4.52$  Hz), 4.84 (s, 1H), 4.97 (t, 1H,  $J = 5.27$  Hz), 5.21 (s, 1H), 5.41 (dd, 1H,  $J = 5.02$  and 9.54 Hz), 6.91 (m, 1H), 6.99 (dd, 1H,  $J = 1.0$  and 8.53 Hz), 7.48 (m, 1H), 7.87 (dd, 1H,  $J = 1.51$  and 8.03 Hz), 10.58 (s, 1H).  $^{13}\text{C}$  NMR ppm ( $\text{CDCl}_3$ ): 14.7, 35.5, 70.2, 73., 74.4, 77.5, 80.5, 85.9, 111.4, 117.2, 118.9, 129.5, 135.6, 154.6, 161.2, 168.9.

**2-(Dimethylaminocarbonyloxy)- 5-O-(*o*-Benzyloxy-benzoyl)-1,4,3,6-dianhydro-D-glucitol.** Compound **17** (0.5612 mmol, 200 mg) and dimethyl carbamoyl chloride (2.2448 mmol, 241.4 mg, 0.2067 mL) was reacted according to GP3. Purification by column chromatography, using ethyl acetate and hexane (3:1, 2:1, 1:1) as eluent, yielded the target compound as a clear oil (186.2 mg, 77.6%).  $^1\text{H}$  NMR  $\delta$  ( $\text{CDCl}_3$ ): 3.88 (dd, 1H,  $J = 6.03$  and 10.04), 3.93–4.05 (m, 3H), 4.57 (d, 1H,  $J = 4.52$  Hz), 4.97 (t, 1H,  $J = 5.02$  Hz), 5.11 (s, 1H), 5.19 (s, 2H), 5.37 (dd, 1H,  $J = 6.03$  and 11.55 Hz), 6.97–7.07 (m, 2H), 7.27–7.55 (m, 6H), 7.91 (dd, 1H,  $J = 1.50$  and 8.03).  $^{13}\text{C}$  NMR ppm ( $\text{CDCl}_3$ ): 35.5, 35.9, 69.8, 70.1, 73.2, 74.0, 78.5, 80.3, 85.7, 113.1, 119.3, 120.1, 126.7, 127.4, 128.1, 131.8, 133.4, 136.1, 154.9, 157.9, 165.3.

**2-(Dimethylaminocarbonyloxy)- 5-O-Salicyloyl-1,4,3,6-dianhydro-D-glucitol (19).** Hydrogenation of its benzyl protected precursor in the presence of palladium on carbon gave **19** as a clear oil (73.8 mg, 62.3%).  $^1\text{H}$  NMR  $\delta$  ( $\text{CDCl}_3$ ): 2.90 (d, 6H,  $J = 15.1$ ), 3.95–4.08 (m, 4H), 4.57 (d, 1H,  $J = 4.52$  Hz), 4.99 (t, 1H,  $J = 5.02$  Hz), 5.19 (s, 1H), 5.41 (q, 1H,  $J = 5.52$  and 10.04 Hz), 6.91 (m, 1H), 7.00 (d, 1H,  $J = 8.53$  Hz), 7.48 (m, 1H), 7.88 (dd, 1H,  $J = 1.51$  and 7.53 Hz), 10.59 (s, 1H).  $^{13}\text{C}$  NMR ppm ( $\text{CDCl}_3$ ): 35.5, 35.9, 70.1, 73.4, 74.4, 78.1, 80.5, 85.9, 111.4, 117.2, 118.9, 129.5, 135.6, 154.8, 161.3, 168.9. HRMS ( $M + 23$ ):  $\text{C}_{16}\text{H}_{19}\text{NO}_7\text{Na}$  requires 360.1054; found 360.1059.

**Determination of Enzyme Activity and Inhibition. Cholinesterases.** First, 1 M solutions of each inhibitor were prepared in 10 mL of acetonitrile/distilled water (1:1) [25  $\mu\text{L}$  of a 1 M inhibitor solution in 250  $\mu\text{L}$  of test solution (see below) gave an inhibitor concentration of 100 mM]. All materials were purchased from Sigma Aldrich Ireland. Then butyrylthiocholine iodide (BTCl)/BTCl (15.9 mg) was dissolved in 10 mL of phosphate buffer pH 8.0 [25  $\mu\text{L}$  of this solution in 250  $\mu\text{L}$  of test solution will give a concentration of 0.5 mM]. ATCl (14.5 mg) was dissolved in 10 mL of phosphate buffer pH 8.0 [25  $\mu\text{L}$  of this solution in 250  $\mu\text{L}$  of test solution will give a concentration of 0.5 mmol]. For human plasma BuChE, human blood samples were collected by venipuncture into Li-Heparin Sarstedt Monovette tubes (9 mL). Plasma was obtained by centrifugation at 10000 rpm for 5 min. Plasma was stored at 2–6 °C. A plasma solution for the activity/inhibition assay was prepared by diluting 1 mL of plasma to 20 mL with phosphate buffer pH 8.0. HuBuChE activity was measured in replicate samples using the basic methods of Ellman et al.,<sup>29</sup> modified in order to allow use of a 96-well plate reader. The total volume of test solution in each well was 250  $\mu\text{L}$ . This consisted of 25  $\mu\text{L}$  of plasma solution, 175  $\mu\text{L}$  of phosphate buffer pH 8.0, 25  $\mu\text{L}$  of DTNB solution [0.5 mmol], and 25  $\mu\text{L}$  of MeCN/distilled water (1:1). The 96-well plate was incubated for 30 min before 25  $\mu\text{L}$  of BTCl solution [0.5 mmol] was added, and the reaction was measured at 412 nm over 5 min using an Anthos bt2 plate reader. For the determination of AChE inhibition: Electric eel AChE (Type VI–S, 1.17 mg) was diluted to 1 mL with phosphate buffer pH 8.0. An aliquot of this (5  $\mu\text{L}$ ) was further diluted to 5 mL (final activity was 0.05–1.15 units  $\text{mL}^{-1}$ ). Enzyme solutions were freshly prepared and used immediately. Then 22  $\mu\text{L}$  of this was diluted to 215  $\mu\text{L}$  with phosphate buffer (pH 8). Test substance (5  $\mu\text{L}$  of 2 mmol in MeCN) was added and the solution incubated at 37 °C for 30 min. To this was added DTNB (27  $\mu\text{L}$ , final concentration 0.3 mmol) and then ACTI (27  $\mu\text{L}$ , final concentration 0.5 mmol).

**Carboxylesterases.** Human microsomal samples were used as enzyme sources for all assays. Pooled human liver microsomes

from male donors were obtained from BD Biosciences (0.5 mL of a 20  $\text{mg}\cdot\text{mL}^{-1}$  solution, lot no. 36170). The sample obtained was diluted in phosphate buffer pH 7.4, producing a stock solution of 2  $\text{mg}\cdot\text{mL}^{-1}$ . To minimize repeated freezing and thawing, the sample was stored in 500  $\mu\text{L}$  aliquots at  $-80$  °C until use. Pooled human intestinal microsomes (lot no. 84921) were obtained as a 20  $\text{mg}\cdot\text{mL}^{-1}$  solution and diluted with phosphate buffer pH 7.4 to a stock concentration of 80  $\mu\text{g}\cdot\text{mL}^{-1}$ . They were stored in 500  $\mu\text{L}$  aliquots at  $-80$  °C until use. The substrate, *para*-nitrophenyl acetate, was obtained from Sigma Ireland.

All assays were carried out in 96-well plates, with the hydrolysis of substrate being monitored by the liberation of chromogenic *p*-nitrophenol at 405 nm with an Anthos Lit-2 absorbance plate reader. The final volume in each well was always 250  $\mu\text{L}$ . It comprised the substrate, dissolved in methanol or acetone to a final assay concentration of 3 mM, 10  $\mu\text{L}$  of the stock microsomal solution, and, where necessary, inhibitors. The remainder of the solution in the wells was 50 mM Tris-HCl buffer pH 7.4. For all assays, the samples to be run included blank reactions in which the substrate alone was dissolved in buffer, as well as positive controls—enzyme and substrate acting in the absence of any inhibitor. The average values for the blank reactions were always subtracted from the test results in order to account for spontaneous hydrolysis of substrate.

When screening for inhibition, compounds were added to each well at a final concentration of 10  $\mu\text{M}$ . Inhibitors were incubated with enzyme at 37 °C for 30 min prior to addition of substrate. The results given are based on four independent measurements.

For  $\text{IC}_{50}$  measurements, each 500  $\mu\text{L}$  aliquot of microsomes was diluted to 3 mL prior to use; 25  $\mu\text{L}$  of this diluted solution were added to each well for testing. Inhibitors (50 nM–200  $\mu\text{M}$ ) were incubated with the enzyme in Tris-HCl buffer pH 7.4 for 30 min prior to addition of substrate and subsequent analysis. For each concentration of inhibitor, four independent measurements were made. The rates of spontaneous substrate hydrolysis, given by blank reactions run alongside each assay, were taken into account in calculations.  $\text{IC}_{50}$  values were obtained directly from sigmoidal concentration response curves to which the data was fit by nonlinear regression (GraphPad Prism5).

**Enzyme Kinetic Analyses.** Wild type human BuChE, obtained as a lyophilized powder, was solubilized in phosphate buffer pH 8.0 for use; D70G and recombinant Y332A and D70G/Y332A mutant enzymes obtained were the kind gift of Dr. Oksana Lockridge, University of Nebraska. The enzymes were used at a final concentration of 0.05  $\text{U}\cdot\text{mL}^{-1}$ , while DTNB and BTCl were used at final concentrations of 0.3 and 0.5 mmol, respectively. All solutions were prepared in phosphate buffer pH 8.0. To monitor enzyme carbamylation over time, a 96-well plate was used, with all assay mixtures being made up to a final volume of 250  $\mu\text{L}$  for monitoring of absorbance at 412 nm. At time 0, 150  $\mu\text{L}$  of inhibitor, at various concentrations, were added to an equal volume of enzyme. Thereafter, at successive time-points, 50  $\mu\text{L}$  aliquots were removed from these wells and added to wells containing 200  $\mu\text{L}$  of DTNB and BTCl in phosphate buffer pH 8.0. Hydrolysis of substrate was monitored by examining the changes in absorbance in each well at 412 nm over the following 30 s. Negative controls were run alongside the test solutions to take account of nonenzymatic hydrolysis, while positive controls gauged the rate of the uninhibited reaction. At least two replicate wells were run for each concentration of inhibitor. A first-order inhibition constant,  $k_{\text{obs}}$  was obtained for each concentration of inhibitor by nonlinear regression to eq 1. The resulting values were fitted to eq 2 using nonlinear regression analysis in order to determine  $K_c$  and  $k_3$ .

The decarbamylation rate constants ( $k_5$ ) were determined by following directly the recovery of the inhibited enzymes subsequent to their inhibition by the tested agents. The enzymes were incubated with each carbamate for at least 1 h at a concentration



that produced more than 85% inhibition. A 1000-fold dilution was made at  $t = 0$  with phosphate buffer pH 8 in order to minimize reinhibition by excess inhibitor. The enzyme was then maintained at a temperature of 37 °C for the remainder of the analysis. Samples were withdrawn at successive time points, and enzyme activity was measured to determine its recovery. Uninhibited enzyme, treated in exactly the same way, was tested at each time point in order to take account of any enzyme degradation over time. Because decarbamylation is a first-order reaction,  $k_5$  was computed from the fit of the data points to a single exponential first-order association curve using the control as a measure of the fully reactivated enzyme.

**Molecular Modeling.** Docking of the carbamate compounds was carried out using AUTODOCK 4, run on Windows XP using the Cygwin engine. A Lamarckian genetic algorithm (LGA) was used in all docking simulations. The inhibitors were built using the builder function of MOE (Chemical Computing Group, Montreal, Canada) and minimized with MOPAC 7 (PM3 method) interfaced to MOE. The protein structure, meanwhile, was the crystal structure of human BChE complexed with a choline molecule (PDB Code 1POM).<sup>13</sup> All nonprotein atoms were removed from the model prior to its use. The missing side chain of residue Gln486 was added in Swiss-PDB Viewer version 3.7 and the missing residues 1–3, 378–379, and 455 added using the “add residue” command in the same program. These added residues were minimized within MOE, with the rest of the macromolecule held fixed. Of the two conformations of the catalytic serine observed in the crystal structure noted above, the one where it makes the anticipated hydrogen bond with His438 was used. His438 was protonated at the  $\delta$  position. The substrates and the enzyme were further prepared for the docking calculation using AutoDockTools 1.4.5. Rotation was allowed for all appropriate bonds in the ligand; the protein was rigid except for the side chains of residues Phe-329, Asp-70, Trp-82, and Phe-398, which were allowed to be flexible during the docking runs. For docking, the 3D affinity grid box was designed to include the full active site gorge of human BChE. The number of grid points in the  $x$ -,  $y$ -, and  $z$ -axes was 64, 64, and 40, respectively, with grid points separated by 0.375 Å. A distance dependent dielectric was used for the modeling of electrostatic interactions. At the beginning of each docking simulation, a population of 300 individuals was randomly selected. During population evolution, a maximum of 25000000 energy evaluations were permitted per generation and 27000 generations were allowed. Just one individual result survived from each generation. Crossover rates and mutation rates were set at 0.8 and 0.02, respectively. In all, 100 docking runs were performed, and the highest scoring pose was taken as being indicative of the correctly docked pose.

**Acknowledgment.** This work was funded by Science Foundation Ireland (05/RFP/CHE0046) and IRCSET (Embark Initiative)

**Supporting Information Available:** Characterization data for compounds **6**, **7**, **8**, **9**, **10**, **11**, **12**, **13**, **14**, **20**, and **21**; elemental analysis data, purity data by HPLC. This material is available free of charge via the Internet at <http://pubs.acs.org>.

## References

- (1) Tago, H.; Maeda, T.; McGeer, P. L.; Kimura, H. Butyrylcholinesterase-rich neurons in rat brain demonstrated by a sensitive histochemical method. *J. Comp. Neurol.* **1992**, *325*, 301–312.
- (2) Manoharan, I.; Kuznetsova, A.; Fisk, J. D.; Boopathy, R.; Lockridge, O.; Darvesh, S. Comparison of cognitive functions between people with silent and wild-type butyrylcholinesterase. *J. Neural Transm.* **2007**, *114*, 939–945.
- (3) Mesulam, M. M.; Guillozet, A.; Shaw, P.; Levey, A.; Duysen, E. G.; Lockridge, O. Acetylcholinesterase knockouts establish central cholinergic pathways and can use butyrylcholinesterase to hydrolyze acetylcholine. *Neuroscience* **2002**, *110*, 627–639.
- (4) (a) Carson, K. A.; Geula, C.; Mesulam, M. M. Electron microscopic localization of cholinesterase activity in Alzheimer brain tissue. *Brain Res.* **1991**, *540*, 204–208. (b) Arendt, T.; Brückner, M. K.; Lange, M.; Volker, B. Changes in acetylcholinesterase and butyrylcholinesterase in Alzheimer's disease resemble embryonic development—A study of molecular forms. *Neurochem. Int.* **1992**, *21*, 381–396. (c) Giacobini, E. Cholinergic function and Alzheimer's disease. *Int. J. Geriatr. Psychiatry* **2003**, *18*, S1–S5.
- (5) Greig, N. H.; Utsuki, T.; Ingram, D. K.; Wang, Y.; Pepeu, G.; Scali, C.; Yu, Q. S.; Mamczarz, J.; Holloway, H. W.; Giordano, T.; Chen, D.; Furukawa, K.; Sambamurti, K.; Brossi, A.; Lahiri, D. K. Selective butyrylcholinesterase inhibition elevates brain acetylcholine, augments learning and lowers Alzheimer beta-amyloid peptide in rodent. *Proc. Natl. Acad. Sci. U.S.A.* **2005**, *102*, 17213–17218.
- (6) Giacobini, E.; Spiegel, R.; Enz, A.; Veroff, A. E.; Cutler, N. R. Inhibition of acetyl- and butyrylcholinesterase in the cerebrospinal fluid of patients with Alzheimer's disease by rivastigmine: correlation with cognitive benefit. *J. Neural Transm.* **2002**, *109*, 1053–1065.
- (7) O'Brien, K. K.; Saxby, B. K.; Ballard, C. G.; Grace, J.; Harrington, F.; Ford, G. A.; O'Brien, J. T.; Swan, A. G.A.; Fairbairn, F.; Wesnes, K.; del Ser, T.; Edwardson, J. A.; Morris, C. M.; McKeith, I. G. Regulation of attention and response to therapy in dementia by butyrylcholinesterase. *Pharmacogenetics* **2003**, *13*, 231–239.
- (8) Diamant, S.; Podoly, E.; Friedler, A.; Ligumsky, H.; Livnah, O.; Soreq, S. Butyrylcholinesterase attenuates amyloid fibril formation in vitro. *Proc. Natl. Acad. Sci. U.S.A.* **2006**, *103*, 8628–8633.
- (9) (a) Lynch, T. J.; Mattes, C. E.; Singh, A.; Bradley, R. M.; Brady, R. O.; Dretchen, K. L. Cocaine detoxification by human plasma butyrylcholinesterase. *Toxicol. Appl. Pharmacol.* **1997**, *145*, 363–371. (b) Morton, C. L.; Wadkins, R. M.; Danks, M. K.; Potter, P. M. The anticancer prodrug CPT-11 is a potent inhibitor of acetylcholinesterase but is rapidly catalyzed to SN-38 by butyrylcholinesterase. *Cancer Res.* **1999**, *59*, 1458–1463.
- (10) (a) Iwasaki, T.; Yoneda, M.; Nakajima, A.; Terauchi, Y. Serum butyrylcholinesterase is strongly associated with adiposity, the serum lipid profile and insulin resistance. *Intern. Med.* **2007**, *46*, 1633–1639. (b) Li, B.; Duysen, E. G.; Lockridge, O. The butyrylcholinesterase knockout mouse is obese on a high-fat diet. *Chem.–Biol. Interact.* **2008**, *175*, 88–91.
- (11) Carolan, C. G.; Dillon, G. P.; Gaynor, J. M.; Reidy, S.; Ryder, S. A.; Khan, D.; Marquez, J. F.; Gilmer, J. F. Isosorbide-2-carbamate Esters: Potent and Selective Butyrylcholinesterase Inhibitors. *J. Med. Chem.* **2008**, *51*, 6400–6409.
- (12) Moriarty, L. M.; Lally, M. N.; Carolan, C. G.; Jones, M.; Clancy, J. M.; Gilmer, J. F. Discovery of a “true” aspirin prodrug. *J. Med. Chem.* **2008**, *51*, 7991–7999.
- (13) Jones, M.; Inkiewicz, I.; Medina, C.; Santos-Martinez, M. J.; Radomski, A.; Radomski, M. W.; Lally, M. N.; Moriarty, L. M.; Gaynor, J.; Carolan, C. G.; Khan, D.; O'Byrne, P.; Harmon, S.; Holland, V.; Clancy, J. M.; Gilmer, J. F. Isosorbide-Based Aspirin Prodrugs: Integration of Nitric Oxide Releasing Groups. *J. Med. Chem.* **2009**, *52*, 6588–6598.
- (14) Carolan, C. G.; Gaynor, J. M.; Dillon, G. P.; Khan, D.; Ryder, S. A.; Reidy, S.; Gilmer, J. F. Novel isosorbide di-ester compounds as inhibitors of acetylcholinesterase. *Chem.–Biol. Interact.* **2008**, *175* (1–3), 293–297.
- (15) Imai, T. Human carboxylesterase isozymes: catalytic properties and rational drug design. *Drug. Metab. Pharmacokin.* **2006**, *21*, 173–185.
- (16) (a) Main, A. R.; Hastings, F. L. Carbamylation and Binding Constants for the Inhibition of Acetylcholinesterase by Physostigmine. *Science* **1966**, *154*, 400–402. (b) Feaster, S. R.; Quinn, D. M. Mechanism-Based Inhibitors of Mammalian Cholesterol Esterase. *Methods Enzymol.* **1997**, *286*, 231–252. (c) Rampa, A.; Piazzini, L.; Belluti, F.; Gobbi, S.; Bisi, A.; Bartolini, M.; Andrisano, V.; Cavrini, V.; Cavalli, A.; Recanatini, M.; Valenti, P. Acetylcholinesterase Inhibitors: SAR and kinetic studies on  $\omega$ -[N-methyl-N-(3-alkylcarbamoyloxyphenyl)-methyl]-aminoalkoxyaryl derivatives. *J. Med. Chem.* **2001**, *44*, 3810–3820.
- (17) Bar-On, P.; Millard, C. B.; Harel, M.; Dvir, H.; Enz, A.; Sussman, J. L.; Silman, I. Kinetic and structural studies on the interaction of cholinesterases with the anti-Alzheimer drug rivastigmine. *Biochemistry* **2002**, *41*, 3555–3564.
- (18) Nicolet, Y.; Lockridge, O.; Masson, P.; Fontecilla-Camps, J. C.; Nachon, F. Crystal structure of human butyrylcholinesterase and of its complexes with substrate and products. *J. Biol. Chem.* **2003**, *278*, 41141–41147.
- (19) Sussman, J. L.; Harel, M.; Frolow, F.; Oefner, C.; Goldman, A.; Tokor, L.; Silman, I. Atomic structure of acetylcholinesterase from *Torpedo californica*: a prototypic acetylcholine-binding protein. *Science* **1991**, *253*, 872–879.

- (20) Nachon, F.; Ehret-Sabatier, L.; Loew, D.; Colas, C.; van Dorsselaer, A.; Goeldner, M. Trp82 and Tyr332 are involved in two quaternary ammonium binding domains of human butyrylcholinesterase as revealed by photoaffinity labeling with [3H]DDF. *Biochemistry* **1998**, *37*, 10507–10513.
- (21) Harel, M.; Schalk, I.; Ehret-Sabatier, L.; Bouet, F.; Goeldner, M.; Hirth, C.; Axelsen, P. H.; Silman, I.; Sussman, J. L. Quaternary ligand binding to aromatic residues in the active-site gorge of acetylcholinesterase. *Proc. Natl. Acad. Sci. U.S.A* **1993**, *90*, 9031–9035.
- (22) Morris, G. M.; Goodsell, D. S.; Halliday, R. S.; Huey, R.; Hart, W. E.; Bewley, R. K.; Olson, A. J. Automated docking using a Lamarckian genetic algorithm and an empirical binding free energy function. *J. Comput. Chem.* **1998**, *19*, 1639–1662.
- (23) Sippl, W. Development of biologically active compounds by combining 3D QSAR and structure-based design methods. *J. Comput.-Aided Mol. Des.* **2002**, *16*, 825–830.
- (24) Bartolucci, C.; Perola, E.; Pilger, C.; Fels, G.; Lamba, D. Three-dimensional structure of a complex of galanthamine (Nivalin) with acetylcholinesterase from *Torpedo californica*: implications for the design of new anti-Alzheimer drugs. *Proteins* **2001**, *42*, 182–191.
- (25) Masson, P.; Froment, M. T.; Bartels, C. F.; Lockridge, O. Asp70 in the peripheral anionic site of human butyrylcholinesterase. *Eur. J. Biochem.* **1996**, *235*, 36–48.
- (26) Masson, P.; Xie, W.; Froment, M. T.; Levitsky, V.; Fortier, P. L.; Albaret, C.; Lockridge, O. Interaction between the peripheral site residues of human butyrylcholinesterase, D70 and Y332, in binding and hydrolysis of substrates. *Biochim. Biophys. Acta* **1999**, *1433*, 281–293.
- (27) Grieg, N. H.; Sambamurti, K.; Quian-sheng, Y.; Perry, T. A.; Holloway, H. W.; Haberman, F.; Brossi, B.; Ingram, D. K.; Lahiri, D. K. Butyrylcholinesterase: its selective inhibition and relevance to Alzheimer's disease therapy. In *Butyrylcholinesterase, Its Functions and Inhibitors*, 1st ed.; Giacobini, E., Ed.; Martin Dunitz: London, 2003; pp 69–90.
- (28) Masson, P.; Bec, N.; Froment, M. T.; Nachon, F.; Balny, C.; Lockridge, O.; Schopfer, L. M. Rate-determining step of butyrylcholinesterase-catalyzed hydrolysis of benzoylcholine and benzoylthiocholine. Volumetric study of wild-type and D70G mutant behavior. *Eur. J. Biochem.* **2004**, *271*, 1980–1990.
- (29) Ellman, G. L.; Courtney, K. D.; Andres, V., Jr.; Feather-Stone, R. M. A new and rapid colorimetric determination of acetylcholinesterase activity. *Biochem. Pharmacol.* **1961**, *7*, 88–95.